REDUCING WINDSHEAR RISK THROUGH AIRBORNE SYSTEMS TECHNOLOGY

Roland L. Bowles
NASA Langley Research Center
Hampton, Virginia

Abstract

Functional requirements for airborne windshear detection and warning systems are discussed in terms of the threat posed to civil aircraft operations. Based on research accomplished to date, a preliminary set of performance criteria for predictive windshear detection and warning systems is defined. Candidate airborne remote sensor technologies based on microwave Doppler radar, Doppler laser radar (lidar), and infrared radiometric techniques are discussed in the context of overall system requirements; and performance of each sensor is assessed for representative microburst environments and ground clutter conditions. Preliminary simulation results demonstrate that all three sensors show potential for detecting windshear, and provide adequate warning time to allow flight crews to avoid the affected area or escape from the encounter. Radar simulation and analysis show that using bin-to-bin automatic gain control, clutter filtering, limited detection range, and suitable antenna tilt management, windshear from "wet" microbursts can be accurately detected. Although a performance improvement can be obtained at higher radar frequency, the baseline X-band system also detected the presence of windshear hazard for a "dry" microburst. Simulation results of end-to-end performance for competing coherent lidar systems are presented. Analysis shows that a Ho:YAG lidar at a wavelength of 2.1 μm and a CO_2 lidar at 10.6 μm can provide the pilot information about line-of-sight component of a windshear threat from his present position to a region extending 2 to 4 km in front of the aircraft, even under conditions of moderately heavy precipitation. Ho:YAG has potentially superior performance to that of the CO_2 lidar, but is not available at this time. Passive infrared techniques show promise, however, more research is needed to establish a proven relationship between temperature measurement and windshear hazards.

1. Background and Introduction

Low-altitude windshear is recognized by the commercial aviation industry as a major hazard. In the United States, during the period 1964 to 1985, windshear has been a contributing factor in at least 26 civil transport accidents and 3 incidents involving 500 fatalities and over 200 injuries. Numerous methods of reducing the low-altitude windshear hazard have been proposed by the airlines, airframe manufacturers, and the Government. The Federal Aviation Administration (FAA), as lead agency for civil aviation safety, has established an integrated windshear program plan which addresses the windshear problem through focused research and development efforts over a multi-year period. The National Aeronautics and Space Administration (NASA) has responded by signing a memorandum of agreement with the FAA (July 1986) to pursue a cooperative research program which addresses technical factors related to airborne detection, avoidance, and survivability of severe windshear atmospheric conditions. Key elements of the NASA research effort include characterization of windshear phenomena in the aviation context, airborne remote-sensor technology that provides forward-looking avoidance capability, and flight-management system concepts that promote risk-reduction piloting through timely and accurate transfer of information to flight crews. The NASA research thrust is directed at developing system concepts which embrace forward-looking sensor technology, thereby providing the flight crew with awareness of the presence of windshear with enough time to avoid the affected area or escape from the encounter.

This paper emphasizes the analysis of candidate sensors for use in an airborne forward-looking detection system, to enable aircraft to avoid the hazards of low-altitude windshear. The analysis includes a definition of sensor performance criteria and functional requirements, the formulation of system concepts to meet these requirements, and an investigation and simulation of the capabilities and limitations of such a system. In order to set a baseline, and establish a point of departure for discussion of advanced airborne system techniques, a review of reactive windshear detection is presented.

Using a microburst/clutter/radar simulation program, a preliminary feasibility study was conducted to assess the performance

Copyright © 1990 by the American Institute of Aeronautics and Astronautics, Inc. No copyright is asserted in the United States under Title 17, U.S. Code. The U.S. Government has a royalty-free license to exercise all rights under the copyright claimed herein for Governmental purposes. All other rights are reserved by the copyright owner.

of airborne Doppler radar for the detection of low-altitude windshear during aircraft takeoff and landing. Preliminary results show that using bin-to-bin automatic gain control (AGC), clutter filtering, limited detection range, and suitable antenna tilt management, windshear from a "wet" microburst can be accurately detected 10 to 65 s (.75 to 5 Km) in front of the aircraft. Although a performance improvement can be obtained at higher frequency, the baseline X-band system simulated also detected the presence of windshear hazard for a "dry" microburst.

The two lidar systems investigated, solid-state Ho:YAG at 2.1 μm and CO_2 at 10.6 μm, appear able to meet the windshear warning requirements as determined by computer simulations of the 1985 Dallas/Fort Worth "wet" microburst event, and as expected, performed well for detecting "dry" microbursts. The performance of Ho:YAG is potentially superior to that of the CO_2 lidar, but Ho:YAG is far from being available at this time. On the other hand, the CO_2 technology is quite mature, and has been tested extensively in both airborne and ground-based windfield mapping applications.

Infrared (IR) radiometers have long been used to measure temperature of remote sources. Measurements indicate that often there is a temperature drop associated with the formation of windshear. Presently, NASA is sponsoring research, under the Small Business Innovative Research Program, to develop airborne IR techniques to detect windshear. Based on a variety of analyses and simulations, IR sensors show promise for detection of windshear 30-60 sec ahead of the aircraft. However, more science is needed to definitively establish relationship between passive temperature measurements and windshear hazards to aircraft.

2. The Threat From Windshear

National attention has focused on the critical problem of detecting and avoiding windshear since the crash on August 2, 1985, of Delta Air Lines Flight 191, a Lockheed L-1011, at the Dallas/Fort Worth International Airport. Other crashes and near misses caused by windshear have occurred almost annually.

On July 11, 1988, between 2207 and 2213 UTC (16:07-16:13 MDT), four successive United flights had inadvertent encounters with severe microburst windshear conditions while on final approach to Denver Stapleton Airport[1] (DEN), each resulting in a missed approach, and subsequent delay. A fifth flight executed a missed approach without encountering the phenomena. All of the flight crews were trained utilizing the resources of the Windshear Training Aid. There was no damage to aircraft and no passenger injuries. At the time the aircraft encountered the microburst, the Terminal Doppler Weather Radar (TDWR) Operations Test and Experiment (OT&E) was in progress and detected divergent flow that intersected the operating zones for the approach runways. The circumstances associated with the July 11, 1988 event, and several other recently documented near misses, suggest that the exposure to windshear risks have not diminished.

The hazard of windshear arises principally from its deceptive nature: In a windshear situation, from a microburst or any other source, the pilot may be confronted with a performance-increasing headwind, followed a few seconds later by a powerful, performance-decreasing tailwind. To cope with the headwind, the pilot may take actions to prevent the plane from climbing. These actions are then compounded by performance loss caused by the tailwind and downdraft, so that it may be impossible to avoid ground impact. The downburst shown in Figure 1 can be entirely invisible to the pilot and the ground controllers, and it need not be associated with any rain on the ground. In a NASA/FAA study of 186 windshear occurrences in 1983, the average change in wind speed was approximately 40 knots.[2]

The NASA/FAA Joint Airport Weather Study (JAWS)[2] observed and measured windshears at the Denver/Stapleton Airport over a 3-month period. The principal finding confirmed that "... low-altitude wind variability (or windshear) presents an infrequent but highly significant hazard to aircraft landing or taking off." From analysis of aircraft accidents where low-altitude windshear was a factor, it appears that the greatest hazards are caused by downdrafts and outflows produced by convective storms.

Pilots now receive inconsistent windshear warnings that are of questionable reliability. Ground systems detected the Dallas microburst a full 2 minutes after Flight 191 crashed. The *Windshear Training Aid*[3] produced by the FAA Integrated Program in 1986, carries the warning, "Maximum windshear capability of jet transports at heavy weight, for a windshear encounter at a critical location, is 40 to 50

knots wind-speed change. Some windshears cannot be escaped successfully [once they are actually entered]!". For this reason it is essential to emphasize avoidance rather than recovery. An onboard forward-looking windshear-avoidance system can warn the pilot, at the location marked "windshear entry" in Figure 1, that he is approaching a wind hazard. When the plane is at the location "recover or crash," it can be too late to inform the pilot that he is in windshear.

3. Requirements for an Airborne Windshear Detection System

3.1 System Definitions

The following definitions provide a contrast of system capabilities given current knowledge and technology maturation for airborne windshear sensing techniques.

• Reactive Windshear Alerting System: A system which senses (in situ) and identifies the presence of windshear after the phenomenon is encountered. Does not inherently provide flight guidance.

• Predictive Windshear Detection and Avoidance System: Systems which sense (remotely) and identify windshear before the phenomenon is encountered.

A. Forward-Looking Detection and Warning System: A system which senses and identifies windshear before, but in close proximity of, an encounter.

B. Forward-Looking Avoidance System: A system which senses and identifies windshear far enough in advance of a possible encounter to allow the crew to consider maneuvering away from the affected area. Such a system shall include display(s) to assist the crew with identification of the hazardous area.

• Airborne Windshear Flight Guidance System: A system which provides the crew with flight guidance to improve recovery probability in a windshear encounter.

• Airborne Windshear Auto Recovery System: A system which integrates or couples autopilot and the autothrottle systems of the aircraft with an airborne windshear flight guidance system.

• Airborne Windshear Situational Display: A display which presents pertinent windshear information such as flight path angle and stall margins. May be available in conjunction with alerting, guidance and/or predictive detection/avoidance system. Windshear severity information may be supplied to the crew on a continuous basis. Does not provide flight guidance information.

3.2 Alert Definitions

Consistent with accepted "quiet dark cockpit concepts," flight crew should receive the lowest level of windshear alert based on time criticality, hazard severity, and phase of flight considerations.

• Windshear Advisory Alert: An alert which is set at a windshear level requiring crew awareness and may require crew action.

• Windshear Caution Alert: An alert which is set at a windshear level requiring immediate crew awareness and subsequent corrective action.

• Windshear Warning Alert: An alert which is set at a windshear level requiring immediate corrective action by the crew.

• Windshear Time-Critical Executive Alert: An alert which is set at a windshear level requiring immediate, unconditional corrective or compensatory crew action, usually consisting of a flight path maneuver.

• Nuisance Alert: An alert which occurs when phenomena is encountered which exceeds the design windshear alert threshold of the system but does not in fact endanger the aircraft. (Examples, turbulence, gust fronts, thermals)

• False Alert: An alert which occurs when the design windshear threshold conditions do not exist. (Examples, fixed and moving ground clutter)

3.3 Functional Requirements

Ideally, there are five distinct functional requirements inherent to the design of airborne windshear protection systems. The first, and clearly the most fundamental, is the detection of scales of atmospheric motion (intensity and duration) that are hazardous to aircraft and to reliably reject those scales of motion which pose no particular threat to aircraft performance. Secondly, the capability of a system to locate position and track movement of hazardous airmass volumes is fundamental to flight safety. The classification of windshear disturbances as to type e.g., gust

front, low-level jet, boundary layer shear, microburst etc., would be useful, however, technology to accomplish this with airborne sensing techniques is not on the immediate horizon. Third, the system must compute windshear severity based on measurement of relevant atmospheric state variables, and employ proven relationships and scaling between the atmosphere and its effect on aircraft performance degradation. Fourth, hazardous conditions must be annunciated to flight crew if computed windshear severity exceeds the system design threshold. Annunciation of advisory, caution and warning information should conform to accepted flight deck design protocol given the time criticality of the alert, hazard severity, and phase of flight. Last, but not least, a fully capable airborne windshear protection system should provide crew displays of relevant situation information regarding proximity of hazard, as well as, relative intensity (severity) and areal or volumetric extent of the hazard.

3.4 Operational and Performance Criteria for Predictive Systems

The fundamental requirement for a forward-looking, airborne windshear detection system is real time remote sensing. This implies the ability to reliably measure line-of-sight and vertical components of wind velocity. The system should monitor the approach path, the runway, and the takeoff path, in both rain and clear-air conditions. An alert should be provided with enough warning time to allow the pilot to safely transit or avoid the windshear or microburst phenomena. If hazardous conditions exist, a windshear warning alert should be annunciated at time t, indicating a predicted decreasing performance shear (aircraft energy loss exceeding design threshold) which the aircraft would experience at $t+\tau$, assuming no evasive maneuvers were taken to avoid the affected area. Displays should be provided to depict range/azimuth velocity structure and/or hazardous air mass volumes including spatial orientation with respect to aircraft, and relative intensity or severity. Specific operational criteria are listed below.

- Computed windshear severity shall include aircraft energy change based on measurement of horizontal shear and vertical wind, in whatever combination they appear; filtered for turbulence, fixed and moving ground clutter, and apparent windshear residue induced by maneuvering flight.
- Hazard identification shall be based on exceedance of design threshold over a specified minimum areal and/or volumetric extent.
- System shall detect windshear in both "dry" (clear air) and "wet" meteorological conditions with ability to detect both heavy and light precipitation microbursts.
- System shall scan approach path, runway and departure corridor consistent with safety requirements for worst case conditions of aircraft crab and drift angles.
- System shall respond in real time with low nuisance and false alarm rate.
- System shall not produce EMI which adversely impacts other aircraft or ownship avionics.
- System shall not produce electromagnetic emissions harmful to people and wildlife.
- System shall operate with minimum maintenance in aircraft environment.

Key performance criteria are presented in Table 1. The preliminary quantitative performance requirements listed in the table are based on research accomplished to date, and should be viewed as design targets.

Table 1 Quantitative Performance Requirements

Provide a minimum of 20 - 40 sec (sensing range ≈ 2 - 4 Km) advance warning to the pilot over operational range of WX conditions	
Provide advisory information on windshear conditions 40 - 80 sec (4 - 8 Km)	
Wind Velocity Resolution	≤ 1 m/s (2 Kts)
Range Resolution	≤ 300 m
Hazard Resolution	≤ 10% of design threshold
Azimuth Scan	± 20° relative to track
Elevation Scan	TBD° relative to track
Probability of Missed Alert	< .1
Probability of Nuisance Alert	4×10^{-4} per flight hour
Probability of False Alerts and Unannunciated Failure	10^{-5} per flight hour

Inherent to the system requirement outlined above is the notion of a hazard index which relates atmospheric motions such as horizontal shear, downdrafts, and updrafts to aircraft performance capability. A numerical hazard index "F" has been derived[4,5] using both these factors, where F > .1 is considered a potential aircraft hazard. The definition of aircraft hazard is not sensitive to the

technology that is employed to detect it, rather, it is the sensing technology that may be sensitive to the hazard definition. Sensor technology must therefore be conditioned to measure all the relevant atmospheric terms. When this is not possible, the missing atmospheric term must be inferred.

4. Definition of Hazard Index

The key to the development of airborne windshear detection, warning, and avoidance systems is the identification of a hazard index. This index should exhibit a functional dependence on atmospheric states that can be reliably sensed, and scale with available aircraft performance in such a way that the index predicts impending flight-path deterioration. The hazard index must also account for factors such as the statistical nature of the windshear threat, fusion of present position and "forward-looking" sensor capabilities, and the development of objective methods for determining system warning thresholds which consider the potential for nuisance alerts. A hazard index which has the above properties, based on accepted fundamentals of flight mechanics, and current state of knowledge of windshear phenomena, has been derived.

An analysis was conducted which revealed the importance of aircraft energy balance for flight in spatially and temporally varying windfields. This energy-state analysis showed that aircraft motions should be referenced to the accelerated and nonhomogeneous airmass which typifies windshear phenomena. The concepts of airplane total energy and rate of change of total energy are useful in interpreting the impact of windshear on aircraft performance. The airplane total energy is defined as the sum of the air-mas relative kinetic energy and the inertial potential energy. Air-mass kinetic energy is used since only airspeed, not ground speed, describes the airplane's ability to climb or maintain altitude. Inertial potential energy is likewise used since it is altitude above the ground that is useful to the airplane.

Therefore, airplane total specific energy (energy per unit weight), or potential altitude, is defined as:

$$h_p = \frac{E}{W} = \frac{V^2}{2g} + h \qquad (1)$$

where V is airspeed, W is aircraft weight, and h is aircraft altitude. See Figure 2 for definitions of flight path and wind coordinate system. The rate of change of specific energy—also defined as the potential rate of climb of the airplane, assuming negligible energy loss when trading airspeed for climb rate—is given by:

$$\dot{h}_p = \frac{\dot{E}}{W} = \frac{V}{g}\dot{V} + \dot{h}. \qquad (2)$$

When combined with appropriate aircraft equations of motion, the potential rate of climb given by Equation 2 reduces to:

WINDSHEAR "HIT"

$$\dot{h}_p = \frac{\dot{E}}{W} = \left\{ \frac{T - D}{W} - \left[\frac{\dot{W}_x}{g} \cos\gamma_a + \frac{\dot{W}_h}{g} \sin\gamma_a - \frac{W_h}{V} \right] \right\} V; \qquad (3)$$

where (T - D)/W is the ratio of aircraft thrust minus drag to weight, W_x and W_h are the horizontal and vertical wind velocity components, respectively, and γ_a is the flight-path angle relative to airmass.

The dot notation in Equation 3 indicates the substantial derivative with respect to time, since the wind velocity components depend explicitly on aircraft position.

For representative numerical values of windshear gradients, and for flight-path angles compatible with stabilized flight, the hazard index labeled as windshear "hit" in Equation 3 is accurately approximated as

$$F = \frac{\dot{W}_x}{g} - \frac{W_h}{V} \qquad (4)$$

and Equation 3 takes the approximate form:

$$\dot{h}_p = \frac{\dot{E}}{W} = \left[\frac{T - D}{W} - F \right] V. \qquad (5)$$

Equations (4) and (5) explicitly define the quantitative impact of windshear on aircraft energy state and the rate-of-climb capability. The analysis reveals that the rate of change of specific energy (potential climb rate) depends linearly on a nondimensional parameter F, which contains only information regarding air mass movement. Further analysis indicated that the subject parameter can be physically interpreted as the loss or gain in available excess thrust-to-weight ratio due to downdrafts, updrafts, and horizontal windshear, thus providing an aircraft-specific index on which to base annunciated warnings.

The derived hazard index given by Equation 4, referred to as the F-factor, exhibits the following properties:

1. It scales with available aircraft performance in such a way as to predict impending flight-path deterioration.

2. It shows a functional dependence on atmospheric states that can be reliably sensed.

3. It is applicable to both in situ and remotely sensed windshear information.

Positive values of F indicate a performance-decreasing situation for the aircraft, whereas negative values indicate a performance-increasing condition due to atmospheric disturbance. Considering jet transports in take-off configuration and the current state of knowledge regarding windshear phenomena, typical numerical values for the terms under hazardous conditions making up the F-factor are:

$$0.1 \leq \frac{T - D}{W} \leq 0.3; \left| \dot{W}_x \right| \leq 0.3 \text{ g}; \left| \frac{W_h}{V} \right| \leq 0.25.$$

Note that a headwind loss of $\dot{W}_x = .1g$ (2 knots/s) has the same impact on aircraft performance (F value) as a downdraft W_h = -15 knots (-1500 ft/min), considering a reference airspeed of 150 knots.

Since F-factor is a measure of the instantaneous loss of rate-of-climb (in the case of reactive detection systems) or predicted loss of rate-of-climb due to the windfield along flight path extended and within the field of view of a remote sensor; the measurement is indicative of the loss of escape capability of the aircraft should a windshear avoidance maneuver be necessary. A preset hazard threshold can be incorporated, which, when exceeded below a specified aircraft altitude, provides an alert to the flight crew. Any combination of horizontal windshear and/or vertical wind that results in F less than the threshold value indicates safe aircraft operation in relation to available excess thrust-to-weight ratio for that aircraft. A threshold exceedance that persists for a sufficient period of time warrants the annunciation of a windshear warning, which indicates to the crew that the affected area should be avoided or an escape maneuver should be initiated. The alert and warning threshold is determined by considering the maximum permissible F in relation to available aircraft performance capability while minimizing potential for nuisance warnings. Research indicates that threshold values for F between 0.1 and 0.15 are representative for landing and take-off phases of flight for jet transport aircraft, considering factors such as aircraft type, configuration, and range of gross weights. Analysis suggests average values for windshear F-factor from five aircraft accidents ranged between .2 and .35. These data indicate that, in all cases, the average F-factor exceeded the ability of the airplane at maximum weight, to accelerate in level flight.

The F-factor concept can be extended to forward-looking sensors through utilization of spatial wind measurements along a given line-of-sight direction, a characteristic which is typical for pulsed-Doppler detection and ranging systems. The substantial derivative expressed in Equation 4, assuming a "frozen windfield" hypothesis, can be approximated as:

$$\dot{W}_x = \nabla W_x \cdot V_i + \frac{\partial W_x}{\partial t} \approx \frac{\partial W_x}{\partial X} V \qquad (6)$$

where V_i is the inertial velocity vector of the aircraft.

4.1 F-Factor Correlation With Ground Radar Microbursts Observations

One technique employed to characterize microbursts, using a single Doppler radar, is the measurement of horizontal peak-to-peak wind speed difference between approaching and receding flows, and the distance over which the differential flow occurs. Since F-factor is sensitive to wind rate of change, or equivalently, spatial wind change (see Equation 6), reliable estimates of F from surface Doppler radar observations may be possible.[6] Given horizontal wind characteristics of divergent isolated microburst flow, it is reasonable to expect maximum horizontal shear to occur in a region bounded by the stagnation cone of the flow. Mean shear calculated from $\Delta U/\Delta R$, where ΔU is defined as peak-to-peak horizontal wind speed change and ΔR the distance over which it occurs, will significantly underestimate maximum shear. In the context of aviation this is important, because the majority of aircraft performance decreasing shear is between the velocity peaks of a divergent outflow.

An analysis was conducted to estimate (in the least-squares sense) linear shear in the

central domain of a modeled microburst, along any radial direction containing the flow stagnation point. The flow is assumed axisymmetric, and the circular domain over which shear is estimated has diameter D. The least-squares residual is given by:

$$J = \frac{1}{2}\int_{-D/2}^{D/2} [\beta X - U(x)]^2 \, dx \qquad (7)$$

where β is the shear in sec $^{-1}$ as defined by the slope of the least-squares line, and U(x) is the outflow profile based on a stagnation point flow with surface boundary layer.[7] The residual is minimized by setting the derivative of J with respect to β to zero, then solving for β to obtain:

$$\beta = K\frac{\Delta U}{\Delta R}\left[\left(\frac{\Delta R}{D}\right)^2 - \left(\frac{\Delta R}{D}\right)^3 \frac{\sqrt{\pi}}{2\alpha}\,\mathrm{erf}\left(\alpha\frac{D}{\Delta R}\right)\right] \qquad (8)$$

where K = 4.1925 and α = 1.1212.

The estimate for linear shear given by Equation 8 is appropriate as long as the wavelength (distance between velocity peaks) is at least 2 to 4 times the distance D over which the least-squares fit is applied. Although the result given by Equation 8 assumes axisymmetric flow, the estimate for β is not biased by a type of asymmetry commonly associated with microbursts, when the magnitude of approaching flow is not equal to that of receding flow due to translational movement.

In the equation for F, the vertical flow velocity Wh appears as one of the terms. This measurement is not directly available from single surface-based Doppler radar systems, and is in general difficult to reliably estimate. Assuming that the divergence given by Equation 8 is constant and symmetric in the cylindrical region of diameter D and height h; then the velocity of the flow in the region can be written as:

$$\bar{V} = (\beta x, \beta y, W_h)^T$$

and mass continuity constraint is satisfied if:

$$W_h = -2\beta h. \qquad (9)$$

Using Equation 6 and substituting Equation 9 into Equation 4 provides the desired estimate of F:

$$\langle F \rangle = \beta\left[\frac{V}{g} + \frac{2h}{V}\right]. \qquad (10)$$

The parameter β, as defined by Equation 8, can be calculated from measurements provided by a single surface-based Doppler radar.

F-factors were computed using Equation 10 and compared with radar observations. Parameters chosen for this computation were, D=1 Km, h=100 m, and aircraft airspeed V was assumed to be 75 m/s. Figure 3 shows the computed F plotted as a function of measured $\Delta U/\Delta R$ (peak-to-peak mean shear) for a selected 95 microburst sample. The data sample included 39 microburst cases provided by NCAR and measured during the JAWS program[8], 27 cases were provided by Lincoln Laboratory and measured during the FLOWS project[9], and 29 cases were provided by NOAA and observed during the CINDE project[10]. The horizontal line on the figure indicates the approximate F value where aircraft performance loss becomes critical, and therefore, represents an admissible threshold level for airborne detection and warning systems. The least-squares regression line describing these data are shown on the figure, and demonstrates excellent correlation with measurement. Figure 4 shows a similar plot, but F is plotted against only measured ΔU; all information regarding spatial scale (ΔR) has been removed. As seen in the figure, the data are essentially uncorrelated, suggesting that quantitative information is lost when spatial scale is suppressed. Comparison of Figures 3 and 4 show, as expected, that the hazard index defined by F is sensitive to wind gradient or wind rate; and does not explicitly depend on wind speed differential, indicative of aircraft airspeed loss for fixed controls and power setting. The above analysis provides a useful scaling between a proposed aircraft hazard index and measured microbursts intensities. Figure 5 shows the cumulative number of microbursts (for the selected data sample) that have positive F values that are less than or equal to a given value. For the data sample studied, all had F values less than .27. Approximately 42 percent of the microburst population have F values less than .1, suggesting that not all microbursts are inherently hazardous to aircraft.

4.2 Windshear Hazard Criteria Defined

Based on the above investigation, several windshear accident reconstructions, and numerous case studies involving inadvertent aircraft encounters with severe windshear, the following definitions are offered. A hazardous microburst is defined as any microburst with an average F-factor exceeding .1 over any 1 km segment, or, any microburst with an average horizontal windshear exceeding 10^{-2} S^{-1} over any 1 km segment. In the aviation context hazardous windshear (whatever the source) is present when the average F-factor exceeds .1 over a 1 km segment along the flight path of an approaching or departing aircraft. In general, windshear encounters resulting in sustained exposure of $F \geq .1$ must be avoided, or an escape and recovery maneuver initiated. At this time, application of the above criteria is restricted to approach and departure phases of flight, turbojet transport category aircraft operating under part 121 rules, and airborne detection and warning systems (reactive or forward look).

5. Approaches to Airborne Windshear Detection

5.1 Reactive Systems

Windshear avoidance, based on crew awareness and training, is not expected to be 100 percent effective. Devices which alert windshear, in situ, have been introduced to reduce the hazard of an inadvertent encounter. Depending on crew action, a typical low altitude windshear may result in reduced airspeed and rate-of-climb, which often result in significant altitude loss and possible ground impact. Full performance capability depends on two key factors: timely recognition and appropriate response. Analysis indicates that only 5 to 15 seconds may be available to recognize and respond after the initial windshear encounter.[3] A reactive windshear detection and alerting system can possibly detect a windshear before it becomes apparent to the crew from normal instrument monitoring, thereby allowing more time for corrective action. Reactive systems, which meet FAA regulation requirements, have been developed by U.S. and international manufacturers.

5.2 Microwave Systems

High-power ground-based Doppler radars operating at C-band and X-band are able to measure wind velocity at ranges of 10 to 20 km by measuring the scattered radiation primarily from precipitation, ice crystals, or other debris in the air. Microwave systems receive only minimal returns from dry air. Although windshear is usually associated with violent thunderstorms in the southern United States, 80 percent of the observed windshear events in the Denver study (JAWS) were "dry" at ground level. However, more recent data suggest the percentage of "wet" and "dry" microbursts are more evenly balanced when geographical areas, other than Denver, are considered. A major problem with on-airport radars—and to an even greater extent airborne radars—is the appearance of ground clutter. For the airborne system, the clutter return from the moving terrain along the flight path can have greater amplitude than, and a frequency in the same band as, the hoped-for Doppler return from the wind. In comparing airborne radars with the ground-based systems such as those participating in the successful JAWS measurements, one must take into account the reduction in transmitter power that such an airborne system will have available, as well as the reduced antenna aperture, leading to a beam divergence of several degrees. All these factors have a significant impact on the ultimate achievable signal-to-noise ratio (SNR).

Previous experiments[11] and studies have demonstrated, in a limited way, the capability of airborne Doppler radars to detect the presence of windshear. However, for aircraft landing and takeoff applications, the problems of severe ground clutter, rain attenuation, and low reflectivity levels must be solved. To consider these problems, a microburst/clutter/radar simulation program has been developed to aid in the evaluation and development of airborne Doppler radar concepts. The simulation program incorporates windfield and reflectivity data bases derived from a high resolution numerical microburst model, clutter maps derived from airborne Synthetic Aperture Radar (SAR) backscatter data, and various airborne Doppler radar configurations and signal processing concepts. The program simulates the operation of a Doppler radar located in an aircraft approaching a runway, sensing signal returns from a windshear microburst, and an airport clutter environment.

5.3 Lidar Systems

For more than two decades, optical heterodyne detection has been successfully used to measure the frequency of Doppler-shifted laser light scattered from moving aerosols. This technique has been pioneered by many researchers, including those working with both NASA and NOAA. Although wind-velocity measurements are routinely made with good

accuracy to ranges of more than 10 km in clear air, the range is seriously degraded by rain. The attenuation of radiation in the infrared is approximately 9 dB/km per inch of rain per hour.[12] Thus, a moderate-size airborne lidar system, which may have 3- to 5-km range in clear air, will have its range reduced to 1 km in a rain of 3 in./h, such as one might find in the core of a "wet" microburst.

Since early work in the 1970's there have been many advances in airborne laser velocimetry. James Bilbro, at NASA's Marshall Space Flight Center has successfully measured wind velocity from an aircraft using a modulated CO_2 continuous wave (cw) laser followed by a large high-power amplifier that produced 10 mJ at 10.6 μm.[13] Bilbro's Doppler lidar operates in clear air and has a range of more than 5 km. A compact and reliable laser system has been flight-tested for several years by J. Michael Vaughan of the Royal Signals and Radar Establishment.[14] His lidar used a cw CO_2 laser focused 300 m in front of the airplane to measure backscatter coefficients at many European and American test sites and airports. Vaughan also uses optical heterodyne detection to determine airplane airspeed from the Doppler shift in the laser radiation scattered from aerosols. Because it is a cw focused system, rather than pulsed, it is difficult to extract range information, and its look-ahead is limited to a warning of only a few seconds. In recent years, pulsed transversely excited atmospheric pressure (TEA) CO_2 lasers have been made increasingly reliable for long-term operation. Such a system has been used with good success by R. Michael Hardesty at NOAA to measure wind velocity and map windfields over a 20-km range with lidar system located in a van [15]. From these studies it is clear that similar systems using smaller lasers can be developed for airborne applications.

5.4 Infrared Radiometer

Measurements indicate that there is a temperature gradient associated with the formation of some windshears. It appears that this gradient can be measured by an airborne infrared radiometer. The radiometers which have been used for this purpose measure emission from the 14-μm band of atmospheric CO_2. The technique compares emission from CO_2 in the immediate neighborhood of the aircraft to the emissions from the CO_2 in the air 4 or 5 km away. It is conjectured that the more negative this temperature gradient, the steeper the gust front causing it. Although it appears that radiometers of this type can detect temperature gradients associated with microbursts under favorable conditions, the question of nuisance alarms has not been addressed, since it has not yet been determined what other types of atmospheric phenomena cause similar gradients.

Presently, there are several industry and government initiatives to develop, apply, and evaluate infrared sensor techniques to detect windshear. Since these devices sense only temperature, simple relationships between wind speed and temperature are greatly needed for their successful application.

One such relationship has been empirically developed by NASA [16,17] from numerical simulations of isolated and stationary microbursts. This relationship is

$$U_{max}(t) = 2.5\Delta T_{min}(t) + C \qquad (11)$$

where U_{max} is the peak outflow speed (in units of m/s) within a microburst at time t, ΔT_{min} is the minimum temperature change (in units of °C) from ambient at time t (i.e., the maximum temperature drop), and c is a constant representing the translation speed of the microburst (zero for stationary microbursts). In terms of the peak horizontal velocity change across the microburst, ΔU_{max}, the above relation may be reexpressed as

$$\Delta U_{max}(t) = -5\Delta T_{min}(t). \qquad (12)$$

It is important to note that the above relationships are based not on local values but maximum values within the microburst. Hence, the above relationship should not be applied in a local sense ΔT_{min} and either U_{max} or ΔU_{max} may not necessarily occur at the same location within the microburst. As an example, a sensor that experiences a temperature drop of 5 °C should not expect to simultaneously experience an outflow speed of 12.5 m/s or a velocity change of 25 m/s; but, somewhere within the microburst there should be a peak velocity change of at least 25 m/s. Typically, peak winds usually occur near the forward edge of the microburst outflow at an elevation of about 100 m, while peak temperature drops occur at the ground and near the center of the microburst.

Conformation of these relationships from observational data is difficult, since data with good horizontal resolution is needed up to an elevation of about 100 m. Equation 11 is

similar to Fawbush and Miller's (1954) well known formula for computing maximum thunderstorm gusts from maximum temperature drop. Their formula is

$$\text{Max Gust (m/s)} = 3.5 - 2.47\Delta T - 0.012\,\Delta T^2 + 8.3 \times 10^{-4}\Delta T^3 \quad (13)$$

which was based on surface observations assembled near 62 nonfrontal thunderstorms with moderate to heavy rain. Although this formula is of higher order than (11), its values do not differ appreciably. Assuming c = 0 in (11), the greatest difference between the two formulas occurs for a temperature drop of about 6°C, with Fawbush and Miller's formula indicating about a 4 m/s greater wind speed.

In the absence of good observational data, the validity of (11) and (12) were tested in numerous numerical simulations of isolated and stationary microbursts. Generally the formulas worked quite well, but there were exceptions. The formulas tended to underestimate the strength of the winds for 1) low-reflectivity ("dry") microbursts, 2) microbursts driven by sublimating and melting snow, and 3) in all cases when a ground-based stable layer existed (see Fig. 6). In the latter set of cases, strong outflows were accompanied by little temperature drop or even a temperature warming. Also, the formulas tended to overestimate the wind speeds in cases of decaying thunderstorm outflows. In these cases, significant temperature drops remained at the ground, as spreading outflows weakened with time.

The development and investigation of (11) and (12) have focused on its application to microbursts. In order for the formulas to be practical they must work well in nonmicroburst environments as well. Other meteorological phenomenon associated with temperature changes are:

1. Gust Fronts
2. Sea Breezes
3. Cold Fronts
4. Thermals generated by daytime surface heating
5. Differential surface heating due to albedo variations
6. Cooling of the air above a precipitation wetted ground
7. Cooling associated with cloud shadow effects
8. Temperature changes associated with mountainous terrain

The applicability of (11) and (12) during these events is not yet known.

6. Airborne Radar Simulation and Performance

A preliminary tradeoff and assessment study was conducted to evaluate the performance of airborne Doppler radar sensors to detect hazardous microburst windshear during aircraft landing. Using a preliminary set of performance requirements for the design of forward-looking sensors, a baseline set of radar parameters was developed for use in assessing wind-shear detection performance using a comprehensive radar simulation program. This program includes excellent models of microburst windfields, realistic clutter maps of airports, and accurate models of Doppler radar operation and signal processing.[18] Table 2 lists the range of radar parameter values considered in the feasibility study and which represent state-of-the-art, airborne, Doppler, radar-hardware capability. Also listed is a baseline set of values used in the initial radar simulation case studies.

Table 2 Wind-Shear Doppler Radar Values

Parameter	Baseline value	Tradeoff range
Pulse repetition freq.	3030	2000-5500
Pulse width (TAU) u-s	1.0	1.0-3.0
Max. det. range, km	10	5-10
Range gate resolution, m	150	150-450
Range sampling window, km	1-9	1-10
Max. unambiguous ws, m/s	24	24-45
Wind-speed accuracy, m/s	1.0	.5-2
Operating frequency, GHz	9.3	9.3-15
Antenna diameter, m	.76	.46-.91
Antenna gain, dB	35.5	31-48
Antenna beamwidth, deg	3	.8-5
Sidelobe level, dB	<-25	-20--35
Antenna polarization	Linear H	Dual pol
Ant. tilt angle range, deg	0-2	0-2
Azimuth angle range, deg	+/-21	+/-45
Minimum det. signal, dBz	0	-15-10
Transmitter peak power, kw	2	.2-10
System noise figure, dB	4	3-6
Return sig. dynam. range, dB	70	60-80
Receiver dynamic range, dB	50	45-55
Xmit/rec. phase jitter, d.rms	.5	.1-2
Number of A/D conv. bits	12	10-14
Clutter filter type	2 pole	TBD
Processing technique	PP	FFT, PP

The radar simulation program is a comprehensive calculation of the expected output of an airborne coherent pulsed Doppler radar system viewing a low-level microburst along or near the approach path of the aircraft. Inputs to the program include the radar system parameters and large data files that contain the characteristics of the ground clutter and the microburst. The ground clutter data file

consists of high-resolution (20 m) calibrated SAR data of selected airport areas. The microburst data files provide reflectivity factors, x, y, z wind velocity components, and other meteorological parameters with a resolution of 40 m. This data base is generated by a numerical convective cloud model driven by experimentally determined initial conditions and represents selected time periods of the microburst development.

For each range bin, the simulation calculates the received signal amplitude level by integrating the product of the antenna gain pattern and scattering source amplitude and phase over a spherical-shell volume segment defined by the pulse width, radar range, and ground-plane intersection. The amplitude of the return from each incremental scatterer in the volume segment is proportional to either the square root of the normalized cross section of the ground clutter (from the clutter map) or the square root of the reflectivity factor of the water droplets in the microburst (from the microburst data base).

6.1 Clutter Model and Analysis

A major problem associated with the sensing of microbursts using an airborne Doppler radar is the presence of ground clutter. To assess the magnitude of this problem, an analysis of clutter spectra and clutter-to-signal ratios (CSR) was conducted using ground clutter maps derived from well-calibrated SAR Normalized Radar Cross Section (NRCS) data. A set of clutter maps has been produced for a number of different airports from existing sets of SAR data. The ground clutter model used for the present simulation cases is a high-resolution, X-band SAR map of the Willow Run, Michigan airport area provided by the Environmental Research Institute of Michigan (ERIM). The SAR image files produced by ERIM provided calibrated NRCS data with a resolution of 20 m. In the simulations, the aircraft is positioned at a selected distance from the runway touchdown point on a prescribed glide slope.

The results of this preliminary clutter analysis show that the highest clutter levels (CSR of 30-60 dB) occur where the pulse in the main beam intersects the ground in an urban area for antenna tilt angle of 0 deg.[18] Two significant results are shown by these analyses which can be used to greatly reduce the effects of clutter. First, lower CSR values occur at short ranges in front of the aircraft at range gates where the pulse in the main beam has not touched the ground. At these ranges the clutter is coming primarily from sidelobes, which if sufficiently low will suppress the clutter signals. Second, it is very evident in the data that a significant reduction of clutter occurs when the antenna is tilted up from 0 to 2 deg (relative to glide slope).

Thus, by limiting the range of data processing and employing proper antenna tilt control, it is felt that CSR levels can be kept below 40 dB (well within the dynamic range capabilities of present-day Doppler radar receiver design technology). High pass filtering techniques can then be employed to reduce clutter to acceptable levels. Studies are underway to evaluate filter algorithms which can provide optimum results.

6.2 Microburst Model

Microburst data sets are generated by a numerical model developed at NASA Langley Research Center and documented in reference 19. The model, the Terminal Area Simulation System (TASS), is time dependent, multi-dimensional, non-hydrostatic cloud model consisting of 11 prognostic equations (momentum, pressure, temperature, water vapor, cloud droplet water, cloud ice crystals, rain, snow, and hail). The model also includes sophisticated parameterizations for cloud microphysics, turbulence closure, surface friction, and open lateral boundary conditions, which are essential to a realistic simulation of the microburst phenomenon. The model is initiated with environmental conditions from observed data near microbursts and outputs data for radar reflectivity, wind velocity components, temperature, pressure, water vapor, rainwater, snow, hail, and cloud water. The ability of the model to generate high-resolution microburst data fields with favorable agreement with observed data has been demonstrated (See references 16, 17, and 19-22).

The three-dimensional version of the model has been used to simulate both microburst and parent storm at horizontal grid resolutions of 200 m. Reasonable comparisons have been demonstrated between model and observed data, including flight recorder data from the 1985 DFW microburst case and the Denver, July 11, 1988, case studies.[20, 21]

Even higher resolution simulations have been obtained with the axisymmetric version of the model. Microbursts with grid resolutions of 20 to 40 m are simulated with this version of the model by specifying a distribution of precipitation or radar reflectivity at its top

boundary. The distribution used for initiating the model may be obtained from either observed radar data or the more coarse resolution 3-D model. Obviously this version of the model cannot simulate asymmetric microbursts; but in spite of this limitation, good agreement with observed data has been found in many cases.

For the radar simulation cases discussed in this paper, a typical "wet" microburst and a typical "dry" microburst were selected and used to investigate radar performance at a particular instant of time. Figure 7a shows the reflectivity factors and velocity field of the axisymmetric "wet" microburst used in the radar simulation. The "dry" microburst is similar in form but with smaller dimensions, lower wind speeds, and much lower reflectivity levels (see Fig. 7b). The "wet" microburst data are taken at 11 minutes after initiation of the microburst calculation and the "dry" microburst data are 23 minutes after initiation. The "wet" microburst resembles an axisymmetric version of the August 2, 1985, Dallas-Ft. Worth storm, and the "dry" microburst is based on soundings taken on July 14, 1982, within the JAWS network near Denver.

6.3 Simulated Airborne Radar Performance

For the baseline Doppler radar-sensor configurations modeled, preliminary analyses of the computer simulation case studies show that windshear can be accurately detected 10 to 65 s in front of the aircraft approaching a hazardous microburst positioned on the flight path of landing aircraft. This was accomplished using a bin-to-bin AGC, clutter filtering, limited detection range, and suitable tilt management. The sensor is highly effective for the "wet" microburst where very high SNR and SCR are obtainable due to large reflectivity levels. For the "dry" microburst, with low reflectivity levels, windshear was detected; however, more tradeoff analyses and signal processing studies are needed before the performance for the "dry" microburst case can be fully assessed.

To improve the performance on the "dry" microburst, several system parameters can be changed. These tradeoff studies have been initiated. For example, to illustrate the radar performance at Ku-band, the "dry" microburst case discussed above was simulated using the same set of baseline parameters, except that the operating frequency was changed to 15 GHz and the PRF was changed to 4878 pulses per s. Preliminary results for the Ku-band system with the "dry" microburst indicate that even though the SNR and SCR values are much lower than those with the "wet" microburst, the wind velocity was successfully measured over the hazardous part of the microburst.

The radar simulation program provides for an azimuth scan mode and the generation of simulated displays of several variables of interest. Figure 8 shows black and white copies of simulated (color) display of radial wind velocity and hazard index for the "wet" microburst. The left display shows contour plots of wind velocity. The right display shows the F-factor hazard index, and it clearly indicates that a potential wind-shear hazard lies on the aircraft path. The hazard index measurements shown do not take into account the vertical wind component. Figure 9 shows the same information for the "dry" microburst case. The conditions, illustrated in Figures 8-9, are for an aircraft located 7 km from touchdown on a 3 deg glide slope, radar antenna tilt 2 deg, microburst centered on projected flight path 2 km from the touchdown point, and a radar frequency of 9.3 GHz.

Initial simulations were conducted with a specific airport, selected microburst time instants, and the baseline radar parameters. These simulations clearly show that in realistic situations, downward-looking airborne radar sensors have the potential to detect windshear and provide information to the aircrew that will permit escape or avoidance of hazardous shear situations. Plans are underway to investigate a full range of microburst/clutter environments, conduct extensive tradeoff and optimization studies, and investigate various signal processing and clutter filtering concepts which can provide reliable windshear detection capability.

7. Airborne Lidar Simulation and Performance

A technology analysis and end-to-end performance simulation measuring signal-to-noise ratios and resulting wind velocity errors for competing coherent laser radar (lidar) systems has been made.[23,5] It shows that a Ho:YAG lidar at a wavelength of 2.1 μm and a CO_2 lidar at 10.6 μm can give the pilot information about the line-of-sight component of a windshear threat from his present position to a region extending 2 to 4 km in front of the aircraft. This constitutes a warning time of 20 to 40 seconds, even under conditions of moderately heavy precipitation. Based on these analyses, a Coherent Lidar Airborne Shear Sensor (CLASS), using a Q-switched CO_2 laser at 10.6 μm, is being designed and developed for flight evaluation in early 1992.

The lidar system simulated consists of a pulsed laser focused 3 km in front of the aircraft. The backscattered radiation is then coherently detected to yield the Doppler shift imparted to it by the line-of-sight component of the wind. More than 100 simulations have been run with this program, computing the end-to-end performance of the system. First, the SNR of the system is calculated as a function of range, and then the achievable velocity accuracy as a function of range and SNR is determined. Two baseline sets of parameters were established in evaluating the microburst detection feasibility of the CO_2 and Ho:YAG lidar systems. The starting parameters for the two lidar systems being compared are shown in Table 3.

Table 3 Windshear Doppler lidar parameter values

	Lidar System	
Parameters	Ho:YAG (2.09 μm)	CO_2 (10.6 μm)
Aerosol Backscatter Coeff. at 500 m ($m^{-1} \cdot sr^{-1}$)	1.3×10^{-6}	5.1×10^{-8}
Optical/Detection Efficiency	0.1	0.1
MLS Atmos. Attenuation (dB/Km)	0.16	1.1
Pulse Energy (μJ)	5	5
Pulse Duration (μs)	0.5	2.0
e^{-2} Intensity Beam Diameter (cm)	15	15
Focal Range (km)	3	3
Aircraft Altitude (m)	500	500
Aircraft Velocity (m/s)	100	100
Lidar Elevation Angle (deg)	- 3	- 3
Distance to Microburst Center (km)	4	4
Pulses Averaged	10	10
Maximum Wind Velocity (m/s)	±25	±25
Wide Bandwidth (MHz)	47.8	9.4
Narrow Bandwidth (Mhz)	≈2	≈2
Range Resolution (m)	300	300

7.1 Coherent Laser Radar (Lidar) Model and Analysis

A Monte Carlo computer simulation has been developed which attempts to realistically model the measurement and detection of atmospheric velocity profiles and windshear with an onboard pulsed coherent Doppler lidar system. The simulation allows numerous input parameters which describe the coherent lidar system, the lidar platform and measurement geometry, the atmospheric model, and the signal processing technique. The approach simulated is that of a pulsed laser which is focused 3 km in front of the aircraft and is then coherently detected to yield Doppler shift in light scattered back to the aircraft. Details regarding the models used for the atmospheric extinction coefficient $\alpha(R)$, and the atmospheric aerosol backscatter profiles $\beta(R)$, are found in reference (24). An end-to-end performance analysis of lidar systems illuminating the July 1982 Denver/Stapleton "dry" microburst and the August 1985 Dallas/Fort Worth "wet" microburst was carried out (see section 6.2). Numerous computer runs were made to obtain data on lidar performance (signal-to-noise ratio and velocity error) as a function of aircraft distance from the microburst core, and data against "dry" and "wet" microbursts were compared.

For the baseline Doppler lidar-sensor configurations modeled, preliminary analysis of the computer simulation case studies shows that windshear can be accurately detected 20 to 45 seconds in front of the aircraft approaching a hazardous microburst positioned on the flight path of landing aircraft. A conclusion of this work is that, in order to demonstrate a windshear threat, it is sufficient for a sensor system to determine that there is a performance-increasing wind followed spatially by a performance-decreasing wind, where these changes are of the order of 10 to 20 knots per half kilometer. An initial assumption has been that 30 s of warning time was a requirement of an airborne windshear-detection system. Using the Ho:YAG or CO_2 lidars examined in this study, this warning time is achievable in most, but not all, microburst situations. In the Dallas/Fort Worth microburst, the peak rain rate was 3.85 in./h at the core. Using the lidar equation to calculate SNR's, we find that a 5-mJ CO_2 lidar on board an aircraft 4 km from the core center will be able to penetrate approximately 250 m into the core. This lidar will completely sense the performance-increasing portion of the winds, but only the start of the performance-decreasing winds in the 1985 Dallas/Fort Worth example.

If an aircraft is 2 km from the microburst core center, the CO_2 lidar can penetrate approximately 700 m into the core of the microburst. This increase in penetration allows the lidar to show clearly a significant portion of the performance-decreasing winds. Reducing the look-ahead distance from 4 km to 2 km reduces the warning time to ≈12 s before the aircraft reaches the near "edge" of the microburst.

7.2 Simulated Airborne Lidar Performance

Color CRT displays have been created using the SNR data and the velocity error data from the simulation program. In an azimuth scanning

mode of ±25 deg (in 5-deg increments) the "dry" microburst is clearly delineated in a 50-deg segment of a PPI (plan position indicator) scan for both the CO_2 lidar and the Ho:YAG system. The range resolution is 300 m. Figure 10 shows the performance of both systems against the Denver/Stapleton "dry" microburst. In Figure 10a and 10b we show the radial wind velocity profile measured with each system out to 8 km, from a lidar sensor located 4 km from the core of the microburst. The scan shows performance increasing winds of 7 m/s (blue) followed by performance decreasing winds of 8 m/s (orange). Both systems show the characteristic outflow patterns associated with a microburst. An aircraft entering this microburst could lose 15 m/s (30 knots) of airspeed in about 1 km. Figures 10c and 10d show the F-factor as measured by the two lidars. Red is used to indicate an F-factor greater than 0.1, indicating critical aircraft performance loss. Yellow is used to indicate potential "caution" for F-factors less than -0.09, which arise from rapid increases in performance-increasing winds. The true F-factor profile, derived from the actual wind data input to the simulation program, is shown in Figure 10e, indicating excellent agreement with the measurements of the lidars. Both lidars penetrate the entire microburst and show both negative and positive F-factors, corresponding to performance-increasing and performance-decreasing winds. These measurements do not take account of the vertical component of the wind velocity, and will consequently underestimate some F-factors. Nevertheless, the simulations show a hazard index varying from -0.1, about 3 km in front of the aircraft, to +0.1 at a range of 4 km. In the afternoon of July 11, 1988, four airliners all had serious encounters with such a low-precipitation microburst at Denver/Stapleton Airport.[1] One of these aircraft came within 80 feet of the ground, .75 nautical miles short of runway threshold. One of the prime concerns of this investigation has been to determine whether similar unique signatures could be obtained from "wet" microbursts. Figures 11a and 11b show the penetration and advance warning that can be achieved in a scan of the fully evolved descending column of the "wet" microburst. The wind velocity measurements in Figures 11a and 11b show that neither lidar penetrates the core of the microburst, which comprised more than 2 km of rain averaging 3 in./h. In Figures 11c and 11d, the CO_2 lidar is 3 km from the microburst core and the Ho:YAG is 4 km from the core. The CO_2 lidar detects a potential hazard (F = -0.1) 1.5 km in front of the aircraft, indicated by a yellow caution on the display. A performance-decreasing hazard, F > +0.1, is detected and shown at a range of 3 km, providing at least 30-s warning to the aircraft. The Ho:YAG gives the warning 1 km earlier. At a distance of 3 km, both systems paint red warnings all across the display of the projected flight path. True hazard-index values at 4 km are shown in Figure 11e, again including both radial and vertical components of the wind.

We conclude from these data that both lidar systems can sense a windshear hazard and warn a pilot in a timely fashion, even under conditions where the microburst cannot be fully penetrated by the laser. The superior performance of the 2.1-μm lidar as compared with the 10.6-μm system is due to the several dB/km greater extinction in rain for the CO_2 system.

Lidar appears to be a viable approach to windshear detection and avoidance, even in conditions of moderately heavy precipitation. The technology necessary to design, build, and test a brassboard 10-μm CO_2 lidar is available. The airborne lidar windshear-detection systems analyzed in this program can give the pilot information about the line-of-sight component of windshear threat from his present position to a region extending 2 to 4 km in front of the aircraft. Techniques to measure and display vertical wind components and spatial distribution are a significant part of the windshear problem, and will be addressed in our continuing investigation. Although an eye-safe lidar at 2 μm enjoys some performance advantages, the lasers and detectors for such a lidar have not yet been sufficiently developed to support their use in a near-term system. In the long term, diode-pumped solid-state lidars could well supplant CO_2.

8. A Cursory Look at Infrared Algorithm Performance

In section 5.4, empirical relationships between peak outflow speed of isolated microbursts and maximum temperature drop were discussed. It is tempting to use these relationships, to infer a temperature based F-factor, which can be supported by measurements obtained from airborne passive IR devices.[25] If the temperature change is assumed to occur over the same spatial extent (considering the microburst as a whole) as does the change in wind speed; then the average rate of change of wind from maximum outflow to stagnation at the core, is obtained from Equation 11:

$$\dot{U} = -2.5\ \Delta\dot{T} \qquad (14)$$

There is no reason to believe that Equation 14 is locally valid (see 5.4). Equation 12, combined with the results of section 4.1, shows that downdraft speed can be approximated by a relationship proportional to ΔT (see Equations 8 and 9):

$$W_h = -\lambda\Delta T \qquad (15)$$

where λ depends on altitude above the ground and microburst dimensions. The above results, when substituted into Equation 4, provides a temperature based estimate of F-factor:

$$F \approx -2.5\,\frac{\Delta\dot{T}}{g} - \lambda\,\frac{\Delta T}{V}. \qquad (16)$$

Performance predicted by Equation 16 was compared to F-factors computed from winds derived from aircraft flight data recorders, and NASA model data, for the first aircraft to encounter the July 11, 1988, Denver microburst event.[1] Based on conditions that existed at the time UAL Flight 395 encountered the microburst, the parameter λ was determined to be 1.5 m/s/°C. The flight path temperature profile used in the calculations was obtained from the validated data base generated by the NASA three-dimensional model[22] (temperature drop of 3 °C in microburst core). Figure 12 shows the comparisons of F-factor, plotted as a function of aircraft position east of runway 26L at Denver Stapleton Airport. The temperature prediction of F closely matches the peak wind derived F, but does not continuously track the wind F at every point. In particular the performance increasing entry into the microburst is not predicted, since there is no thermal generating mechanism at that location. The peak values for F agree within 20 percent, and spatial extent of the thermal signature is in good agreement with that of the wind based F. The results of this analysis are encouraging, however, it must be emphasized that the algorithm has not been tested against a representative microburst population for which "truth" data exists.

9. Relative Merits of Reactive and Forward-Look Detection

The performance degradation of lidar in heavy rain, and detection limitations of radar for low reflectivity distributed targets in severe clutter environments, raises several important questions. Key among those questions being what range of forward-look alert times are required to assure aircraft survivability and flight crew acceptance of attendant windshear cockpit automation? A definitive answer to this question is not available at this time, due to complex issues involving human factors, piloting techniques, flight guidance and windshear information display, and consideration of specific aircraft performance capabilities.

The peak F-factor seen in many severe windshears, 0.20 to 0.25, is typically only about twice the climb gradient performance capability of the transport aircraft fleet, 0.10 to 0.18. The average F-factor seen by an aircraft during a microburst encounter may be much closer to the aircraft's climb angle capability. This raises the possibility that go-around maneuvers begun relatively close to a microburst will ensure adequate performance for survival. In order to set the stage for windshear predictive sensor technology development, an effort was undertaken to quantify the performance benefit of early microburst detection and establish a minimum warning time for survival.

The approach to this effort was to perform an analytical study of the change in airplane energy height across a windshear event, as a function of the alert timing, and then validate the results in piloted simulation. The governing equation for the energy height analysis is given in (5). By integrating Equation 5 across a windshear event, the total change in energy height can be estimated. In the case of a reactive alert, alert time less than zero, the integration is from windshear entry to windshear exit. In the case of predictive alerting, alert time greater than zero, the integration is from the time of the alert until windshear exit. Each case assumes a 2 sec delay from the alert to thrust increase and a constant F-factor across a shear width of 1524 m (5000 ft). The value of (T-D)/W prior to the alert was set constant at -0.05 and after the alert a constant value of 0.16 was used. Figure 13 shows the results of this integration for windshears of various intensities. The results indicate that with a 10 to 15 sec delay in detecting a windshear, even a relatively weak shear will result in the loss of 92 to 152 m (100 to 500 ft) of energy height. Alerts given only 15 to 20 sec prior to shear entry permitted recovery from relatively strong shears with essentially no altitude loss. For each second of improvement in the alerting time, the energy height loss across the event was reduced by about 9 to 12 m (30 to 40 ft).

The results of the energy height analysis were substantiated in a piloted simulation of microburst recovery procedures.[26] In that study, which investigated landing approach microburst encounters, three recovery procedures and two alert times were tested. A reactive alerting system was simulated in half the runs by providing an alert 5 sec after a threshold F-factor was exceeded. A predictive sensor was simulated in the other half of the runs by providing an alert 10 sec prior to reaching the region of warning threshold F-factor. The results showed that the minimum altitudes during recoveries increased from an average of 30 m (100 ft) to an average of 121 m (398 ft) when the reactive alert was changed to a predictive alert, yet the performance differences between the three recovery procedures tested was negligible. With 10 sec of predictive warning, and crews that were prepared to execute a recovery immediately upon receiving an alert, the minimum altitude during a run was generally the altitude at which the recovery was begun. Based on these results, it can be concluded that a predictive sensor need only provide alerts 15 to 20 seconds in advance of a windshear encounter to ensure aircraft survival over a representative range of windshear severity.

10. Concluding Remarks

Based on preliminary results of tradeoff and performance assessment studies, all three sensor techniques explored in this paper show potential to detect hazardous windshear conditions. The technology necessary to design, build, and test brassboard systems is at hand.

The airborne systems analyzed in this paper appear capable of providing flight crew with information about line-of-sight component of windshear, from present position to a region extending 2-4 km in front of the aircraft. Once hazardous windshear is detected, the crew must be alerted in a timely manner in order to avoid or escape the hazard. A hazard index has been developed which establishes a relationship between sensor measurements and windshear impact on aircraft performance. Simulation studies demonstrate that airborne Doppler systems (radar, lidar) can detect the horizontal component of this index with sufficient accuracy to annunciate timely warnings. Further studies using this index, and associated threshold criteria, will be conducted to assess missed, nuisance, and false alarm rates.

Finally, there are many questions which can be definitively answered only through a sensor validation flight program. NASA has planned, for the 1990-1993 time period, a series of flight experiments to evaluate and demonstrate an experimental X-band Doppler radar, a 10.6 μm Doppler lidar, and a passive infrared radiometer. Performance data and operational system characteristics derived from this program, will be made available to FAA and industry, to support certification and manufacturing initiatives. Continued collaboration between Government and industry is the only reasonable approach to achieve, full performance, airborne windshear protection in the near future.

Acknowledgements. The work reported here is based on the dedication and outstanding accomplishments of the NASA Langley Research Center Windshear Research Team. In addition, the author would like to thank Langley management advocates of the program for their interaction, probing questions, and support.

References

1. Schlickenmaier, H. W.: Windshear Case Study: Denver, Colorado, July 11, 1988. DOT/FAA/DS-89/19, November 1989.

2. Wilson, J. W.; et al: Microburst Wind Structure and Evaluation of Doppler Radar for Airport Windshear Detection. Prepared for the Joint Airport Weather Studies Project. National Center for Atmospheric Research, Boulder, Colorado. NCAR report JAWS, January 1984.

3. Federal Aviation Administration: Windshear Training Aid. Example Windshear Training Program, February 1987.

4. Bowles R. L.: Windshear Detection, Warning, and Flight Guidance. NASA CP 10004: DOT/FAA/PS-87/2, October 1987.

5. Bowles, R. L.; and Targ, R: Wind Shear Detection and Avoidance: Airborne Systems Perspective. International Congress of Aeronautical Sciences, Jerusalem, Israel, August-September 1988.

6. Elmore, K. L.; and Sand, W. R.: A Cursory Study of F-Factor Applied to Doppler Radar: Third International Conference on The Aviation Weather System, Anaheim, California, January 30-February 3, 1989.

7. Oseguera, R. M.; and Bowles, R. L.: A Simple, Analytic 3-Dimensional Downburst Model Based on Boundary Layer Stagnation Flow. NASA TM 100632, July 1988.

8. Hjelmfelt, M. H.: in press: Structure and Life Cycle of Microburst Outflows Observed in Colorado. Journal of Applied Meteorology, No. 27, 900-927.

9. Wolfson, M. M.; DiStefano, J. T.; and Fujita, T. T.: Low-Altitude Wind Shear in the Memphis, Tennessee Area Based on Mesonet and LLWAS data. Preprints, 14th Conference on Severe Local Storms, Indianapolis, American Meteorological Society, pp. 322-327, 1985.

10. Wilson J. W.; Moore, J. A.; Foote, G. B.; Martner, B.; Rodi, A. R.; Uttal, T.; and Wilczak, J. M.: Convection Initiation and Downburst Experiment (CINDE). Bulletin of the American Meteorological Society, No. 69, pp. 1328-1348, 1988.

11. Staton, L. D.: Airborne Doppler Radar for Wind Shear Detection. In workshop proceedings, Windshear/Turbulence Inputs to Flight Simulation and Systems Certification. NASA CP 2474, July 1987.

12. Chu, T. S.; and Hogg, D. C.: Effects of Precipitation at 0.63, 3.5, and 10.6 Microns. The Bell Systems Technical Journal, May-June 1968.

13. Bilbro, J. W.: Atmospheric Laser Doppler Velocimetry: An Overview. Optical Engineering, Volume 19, No. 4, July-August 1980.

14. Vaughan, J. M.; et al.: Atmospheric Backscatter at 10.6 Microns, a Compendium of Measurements Made Outside the United Kingdom by the Airborne LATAS Coherent Laser Radar Velocimeter. Procurement Ministry of Defense, RSRE, Malvern, Worchestershire, May 1987.

15. Hardesty, R. M.; et al.: Ground-Based Coherent Lidar Measurement of Tropospheric and Stratospheric Parameters. SPIE, Vol. 415, Coherent Infrared Radar Systems and Applications II, 1983.

16. Proctor, F. H.: Numerical Simulations of an Isolated Microburst. Part I: Dynamics and Structure. Journal of Atmospheric Science, No. 45, pp. 3137-3160, 1988.

17. Proctor, F. H.: Numerical Simulations of an Isolated Microburst. Part II: Sensitivity Experiments. Journal of Atmospheric Science, No. 46, pp. 2143-2165, 1989.

18. Bracalente, E. M.; et al.: Airborne Doppler Radar Detection of Low-Altitude Wind Shear. Journal of Aircraft, Volume 27, No. 2, February 1990.

19. Proctor, F. H.: The Terminal Area Simulation System. Volume 1: Theoretical Formulation. NASA Contractor Rep. 4046, NASA, Washington, DC, 176 pp., 1987.

20. Proctor, F. H.: The Terminal Area Simulation System. Volume II: Verification Experiments. NASA Contractor Rep. 4047, NASA, Washington, DC, 112 pp., 1987.

21. Proctor, F. H.: Numerical Simulation of the August 2, 1985 DFW Microburst with the Three-Dimensional Terminal Area Simulation System. Preprints Joint Session of 15th Conference on Severe Local Storms and Eighth Conference on Numerical Weather Pred, Baltimore, Amer. Meteor. Soc., pp. J99-J102, 1988.

22. Proctor, F. H.; and Bowles R. L.: Investigation of the Denver 11 July 1988 Microburst Storm with the Three-Dimensional NASA-Langley Windshear Model. Windshear Case Study: Denver, Colorado, July 11, 1988, DOT/FAA/DS-89/19, 1989.

23. Targ, R.; and Bowles, R. L.: Investigation of Airborne Lidar for Avoidance of Windshear Hazards. AIAA Paper 88-4685. Presented at the AIAA Conference on Sensor and Measurement Techniques for Aeronautical Application, Atlanta, Georgia, September 7-9, 1988.

24. Huffaker, R. M; et al.: Performance Analysis and Technical Assessment of Coherent Lidar Systems for Airborne Wind Shear Detection. SPIE Paper 889-11, January 1988.

25. Adamson, H. P.: Airborne Passive Infrared System for the Advanced Warning of Low-Level Windshear and Clear Air Turbulence: 1988 In-Service and Theoretical Work. AIAA Conference on Sensors and

Measurements Techniques for Aeronautical Applications, AIAA-88-4659, 7 pp., Atlanta, Georgia, 1988.

26. Hinton, D. A.: Recovery Strategies for Microburst Encounters Using Reactive and Forward-Look Windshear Detection. AIAA Paper 89-3325. Presented at AIAA Flight Simulation Technologies Conference, Boston, Massachusetts, August 14-16, 1989.

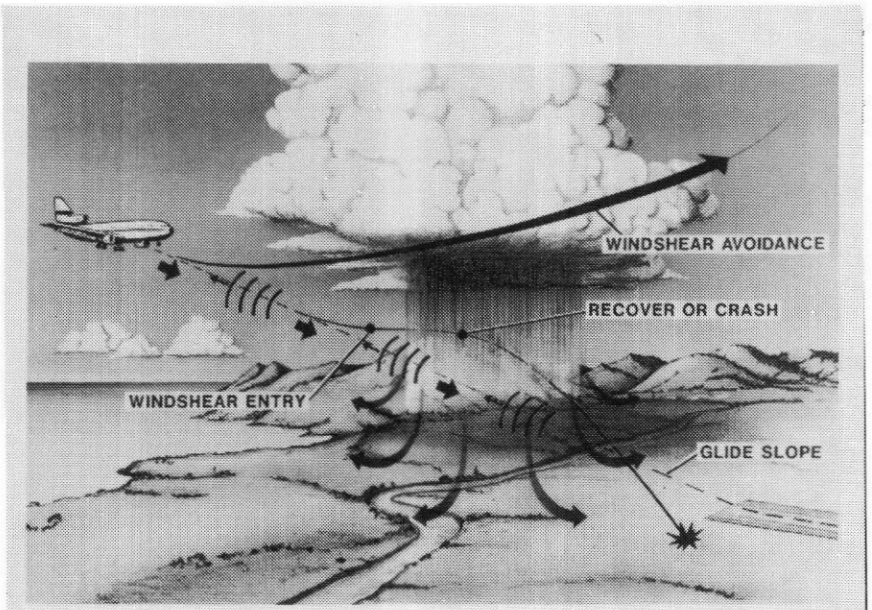

Figure 1. The wind shear problem.

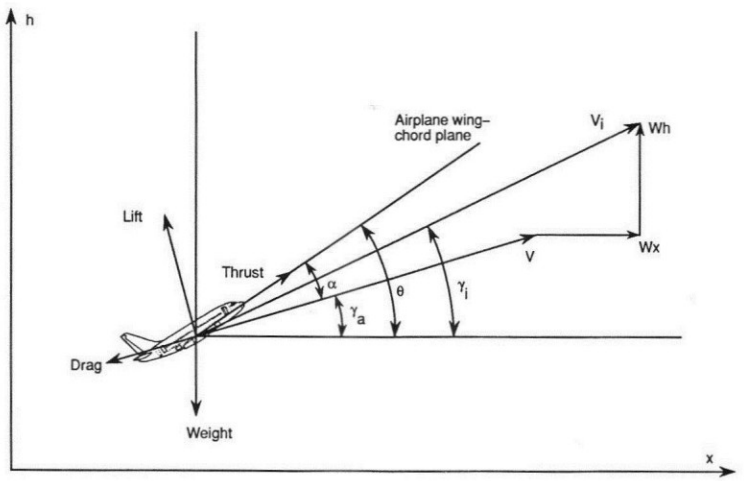

Figure 2. Flight path and wind coordinate system.

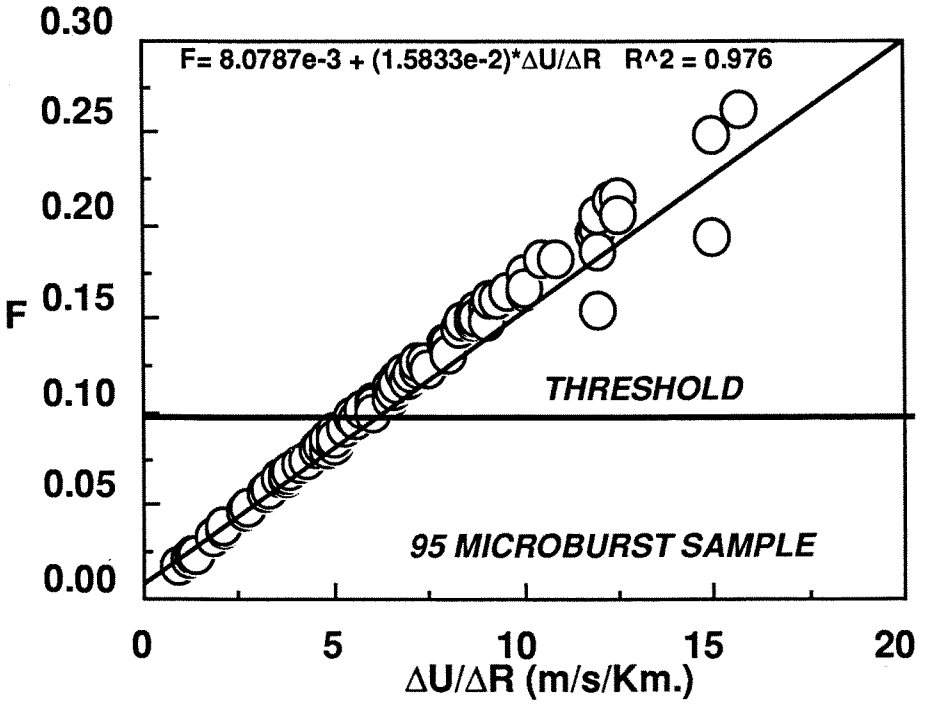

Figure 3. F estimate plotted as a function of ΔU/ΔR for 95 different microburst measurements. The horizontal line shows the approximate F value where jet transport performance loss becomes critical.

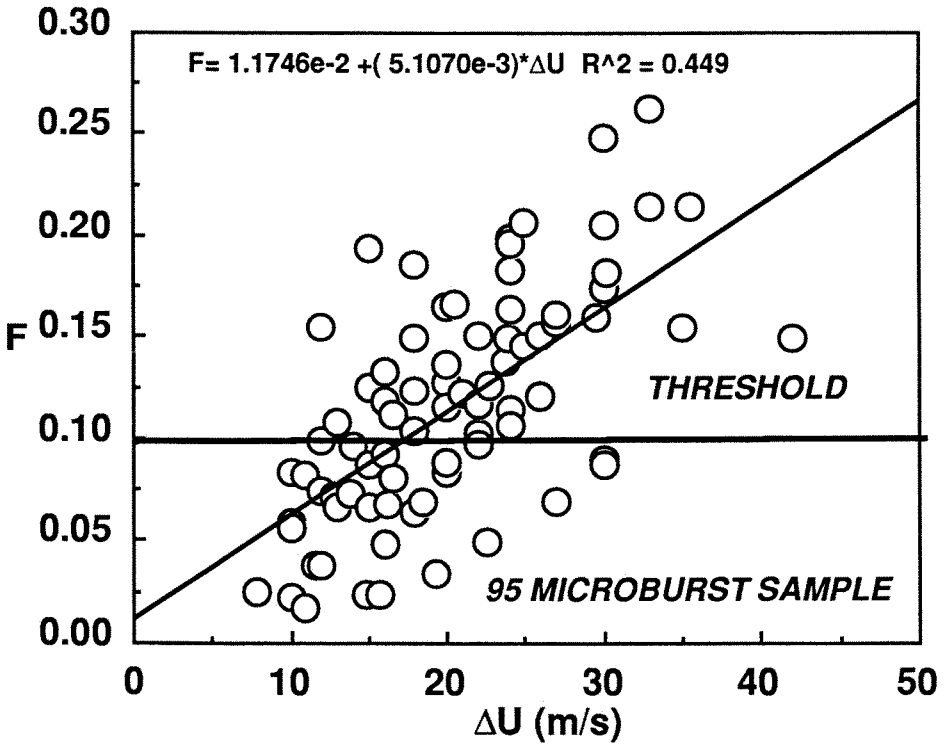

Figure 4. F estimate as a function of measured ΔU for 95 microburst sample.

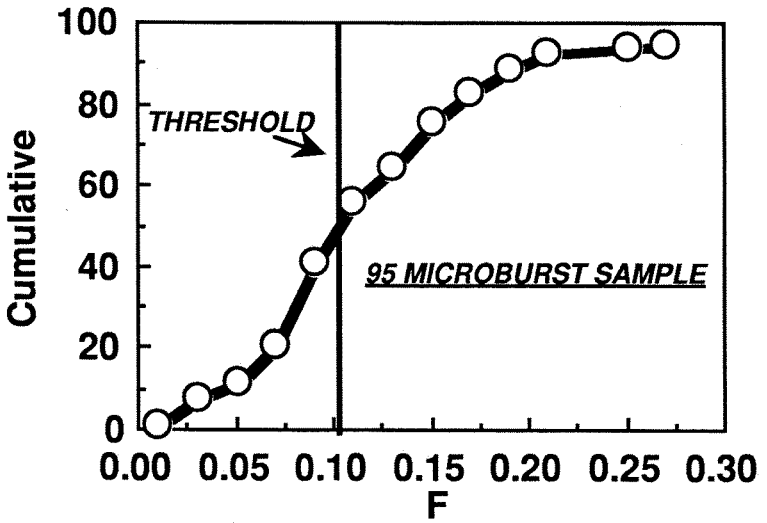

Figure 5. Cumulative number of microbursts with positive F values less than or equal to a given abscissa value.

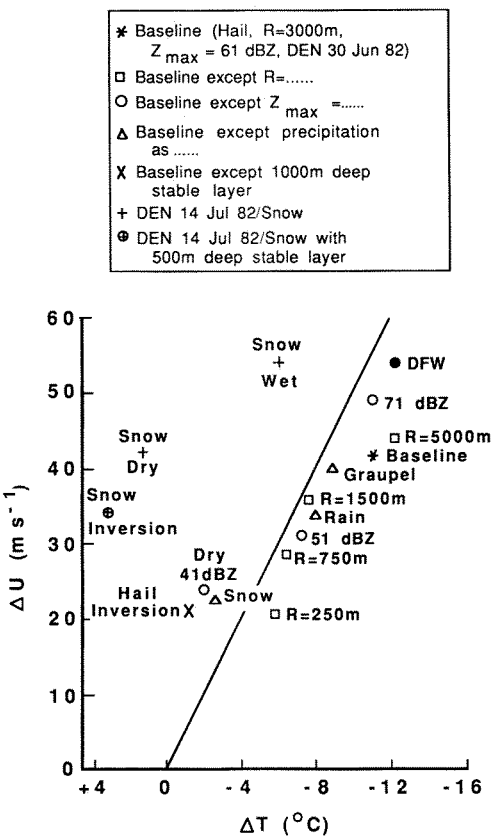

Figure 6. Maximum temperature drop at the ground vs. maximum velocity differential from selected case experiments. The solid line represents $\Delta U = -5\ \Delta T$.

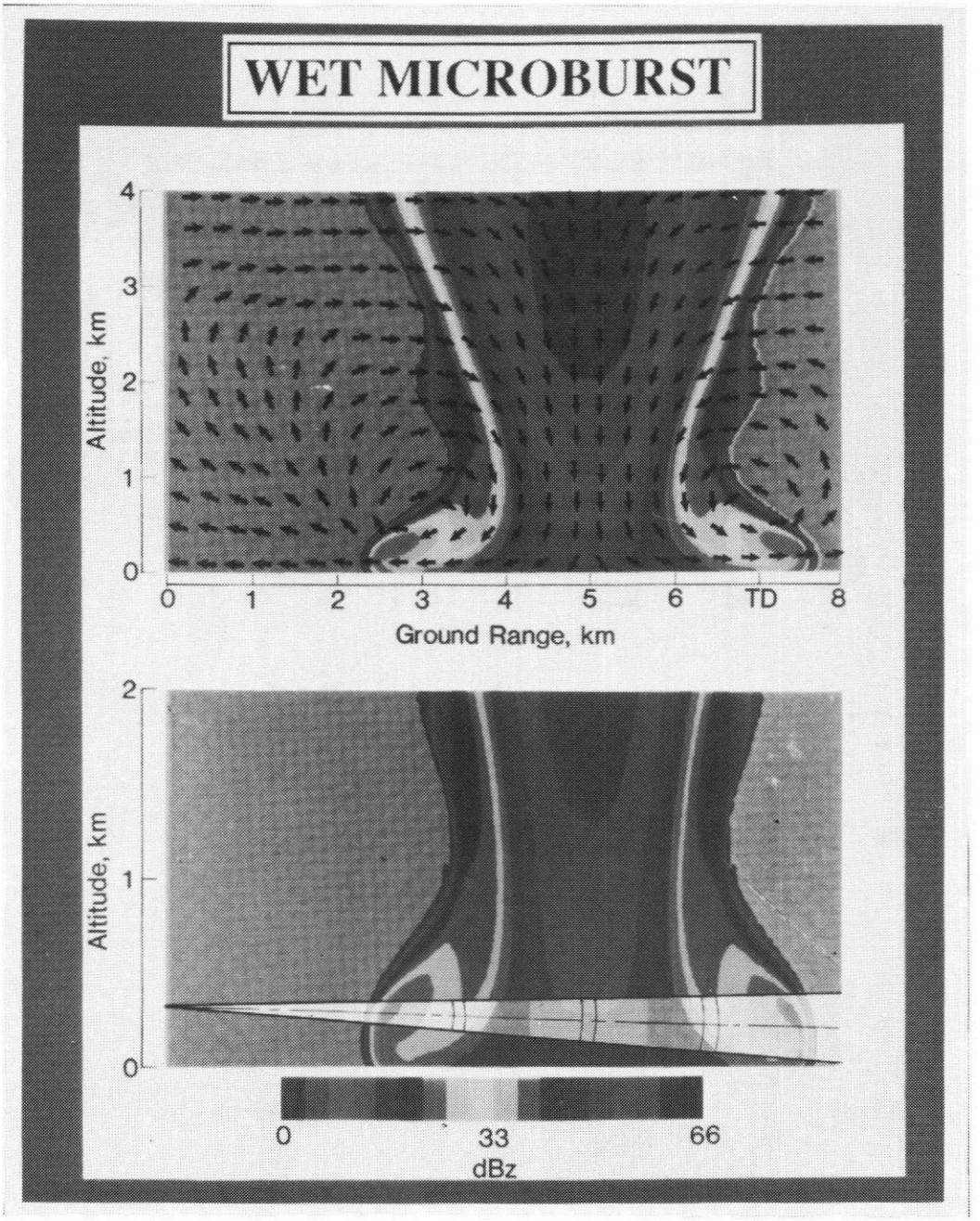

Figure 7 a. Reflectivity contours and velocity field for the axisymmetric "wet" microburst model used for initial radar and lidar performance studies. Lower picture represents expanded view of lowest 2km altitude region (reflectivity only), for an aircraft at 300 m altitude on approach to touchdown point T.D., and a beam divergence consistent with X-band radar frequency.

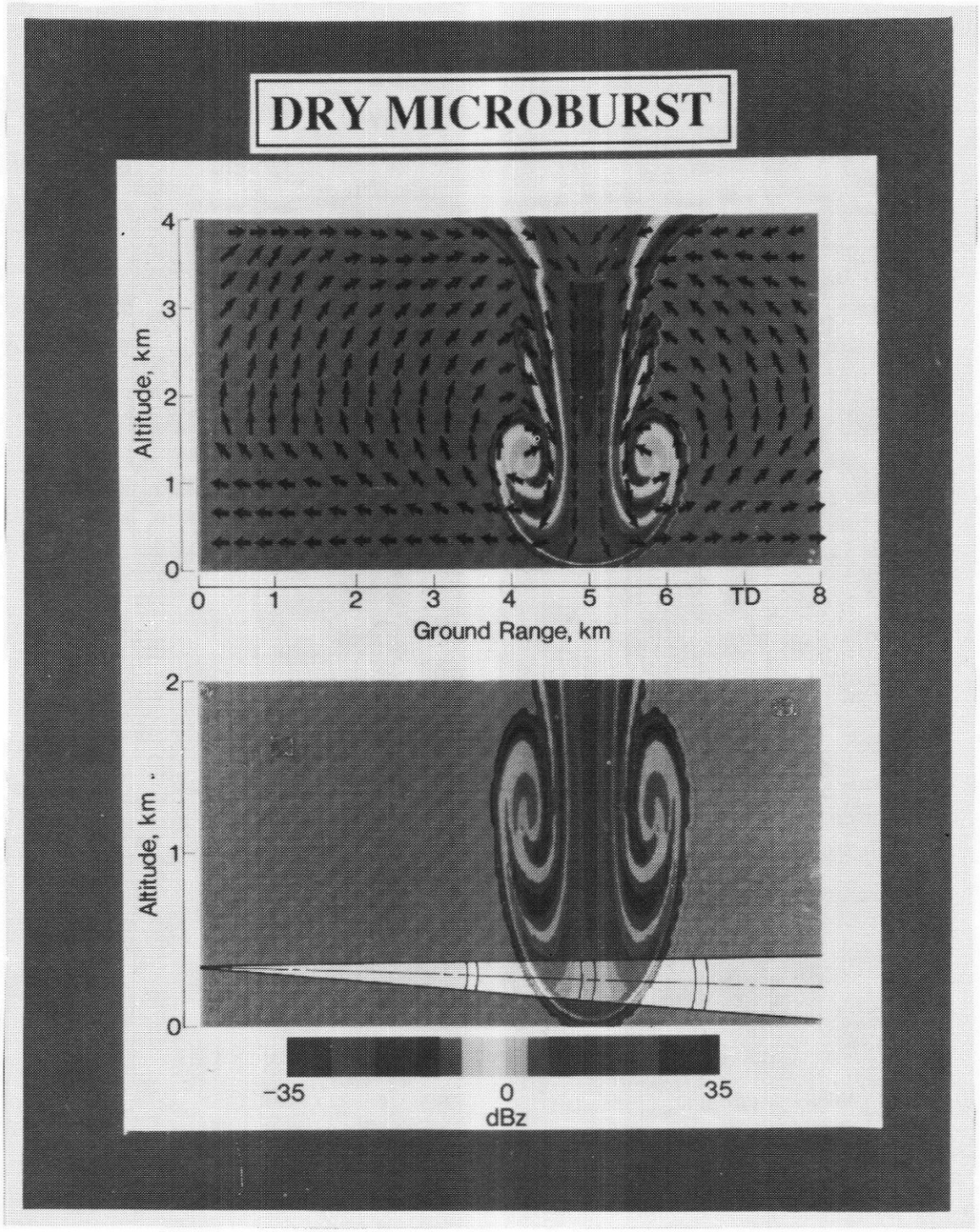

Figure 7 b. Same as figure 7a except "dry microburst case.

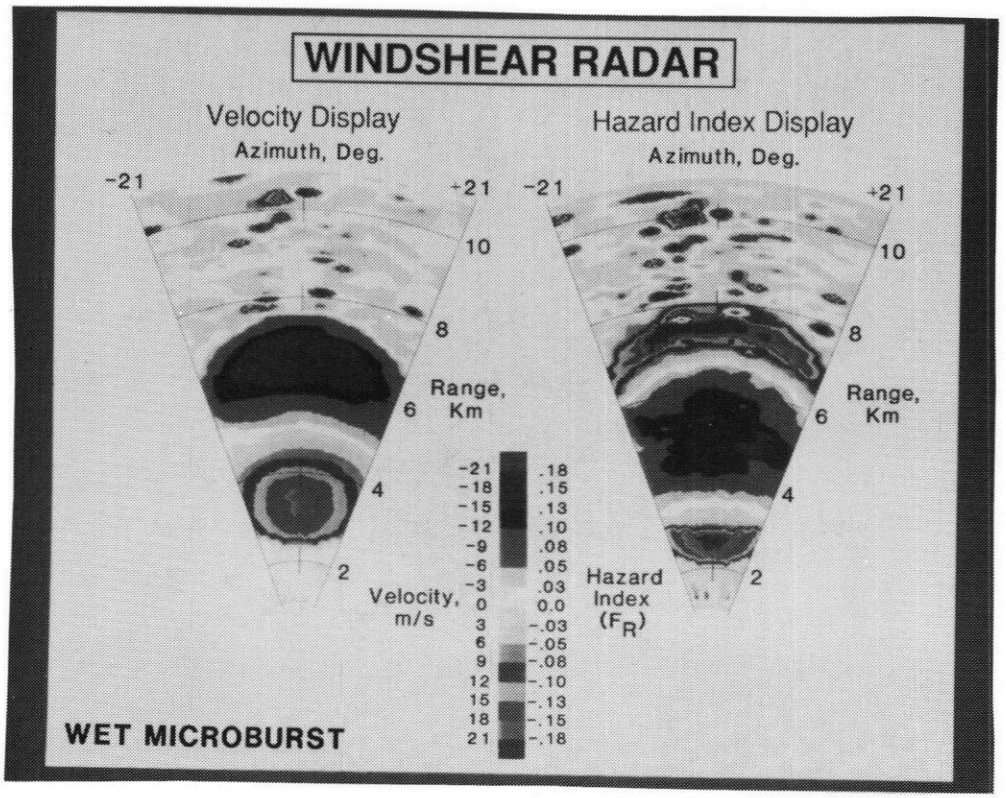

Figure 8. Range-azimuth display of wind velocity and hazard index contours for the "wet" microburst, baseline radar parameters, and conditions listed in the text. the large head-to-tail velocity and wind direction change is clearly shown in the left display. The right display of hazard index clearly shows the potential shear hazard area.

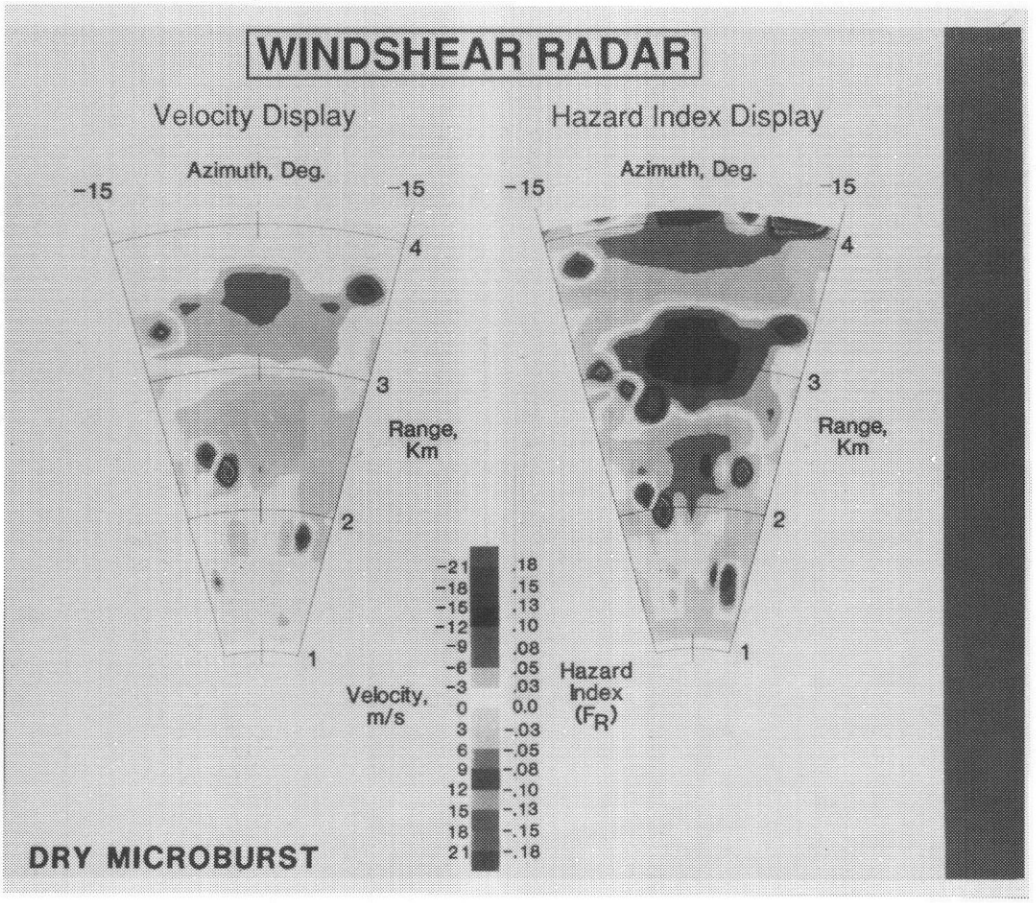

Figure 9. Same as figure 8 except "dry" microburst case and azimuth scan limited to ±15°.

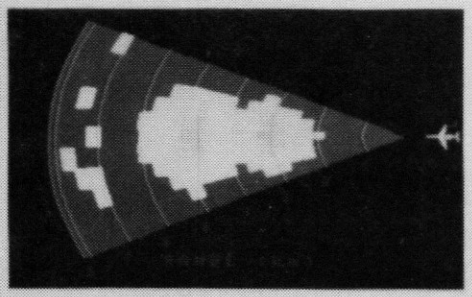

(a) CO_2 lidar wind velocity

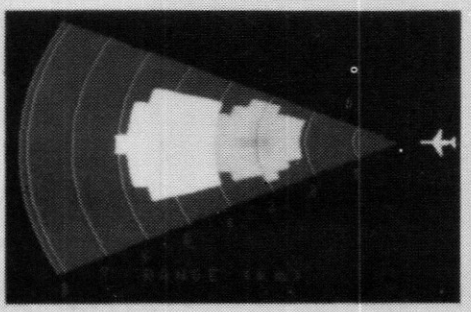

(b) Ho:YAG lidar wind velocity

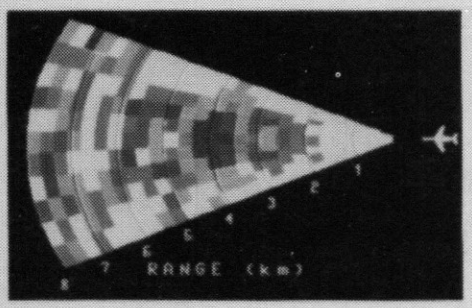

(c) CO_2 lidar hazard index

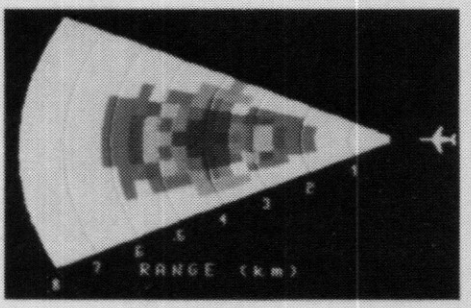

(d) Ho:YAG lidar hazard index

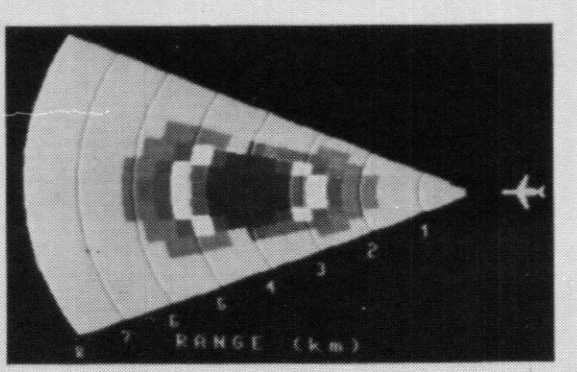

(e) True hazard index

WIND VELOCITY (m/s)

a. RADIAL WIND VELOCITY CONTOURS

RADIAL VELOCITY (m/s)

< -13
-13 < -11
-11 < -9
-9 < -7
-7 < -5
-5 < -3
-3 < -1
-1 < 1
1 < 3
3 < 5
5 < 7
7 < 9
9 < 11
11 < 13
> 13

HAZARD INDEX (red = F-factor > 0.1)

b. HAZARD INDEX

(RED = HAZARD INDEX (F-FACTOR) > 0.1)

HAZARD INDEX F (measured)

F > 0.13
0.11 < F < = 0.13
0.09 < F < = 0.11
0.07 < F < = 0.09
0.05 < F < = 0.07
0.03 < F < = 0.05
0.01 < F < = 0.03
-0.01 < F < = 0.01
-0.03 < F < = -0.01
-0.05 < F < = -0.03
-0.07 < F < = -0.05
-0.09 < F < = -0.07
-0.11 < F < = -0.09
-0.13 < = F

Figure 10. Range azimuth scan of a dry microburst at Denver/Stapleton airport. Simulated wind-velocity measurements are shown for CO_2 lidar in (a) and for Ho:YAG lidar in (b); simulated lidar measurements of hazard index for the two lidars are shown in (c) and (d); the true hazard index is shown in (e), including line-of-sight and vertical components.

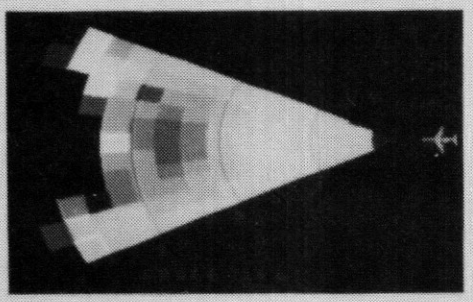

(a) CO_2 lidar wind velocity

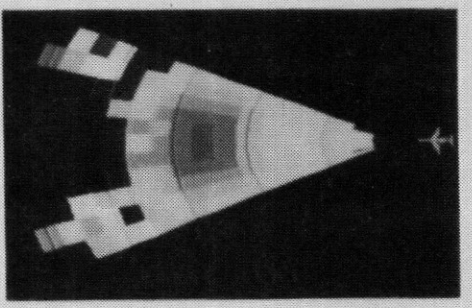

(b) Ho:YAG lidar wind velocity

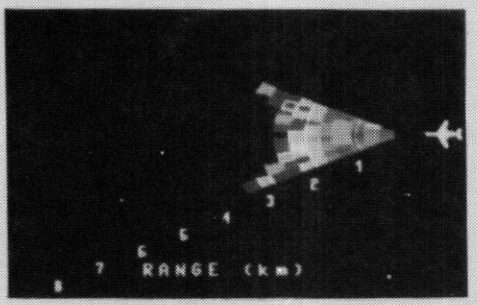

(c) CO_2 lidar hazard index

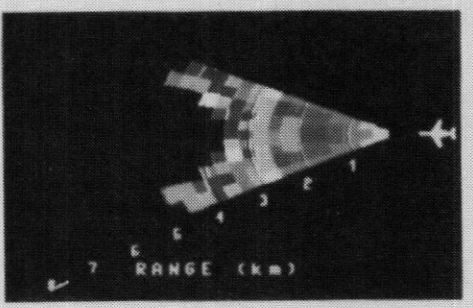

(d) Ho:YAG lidar hazard index

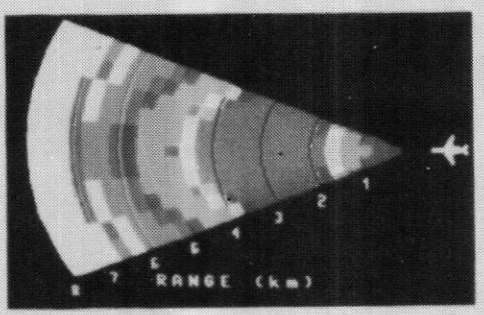

(e) True hazard index

WIND VELOCITY (m/s)

a. RADIAL WIND VELOCITY CONTOURS

RADIAL VELOCITY (m/s)

HAZARD INDEX (red = F-factor > 0.1)

b. TRUE HAZARD INDEX,
RADIAL PLUS VERTICAL F-FACTOR

HAZARD INDEX F (true)

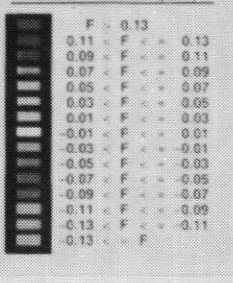

Figure 11. Range azimuth scan of a wet microburst at Dallas/Fort Worth airport. Simulated wind velocity measurements are shown for CO_2 lidar in (a) and for Ho:YAG lidar in (b); simulated lidar measurements of hazard index for the two lidars are shown in (c) and (d); the true hazard index is shown in (e), including line-of-sight and vertical components.

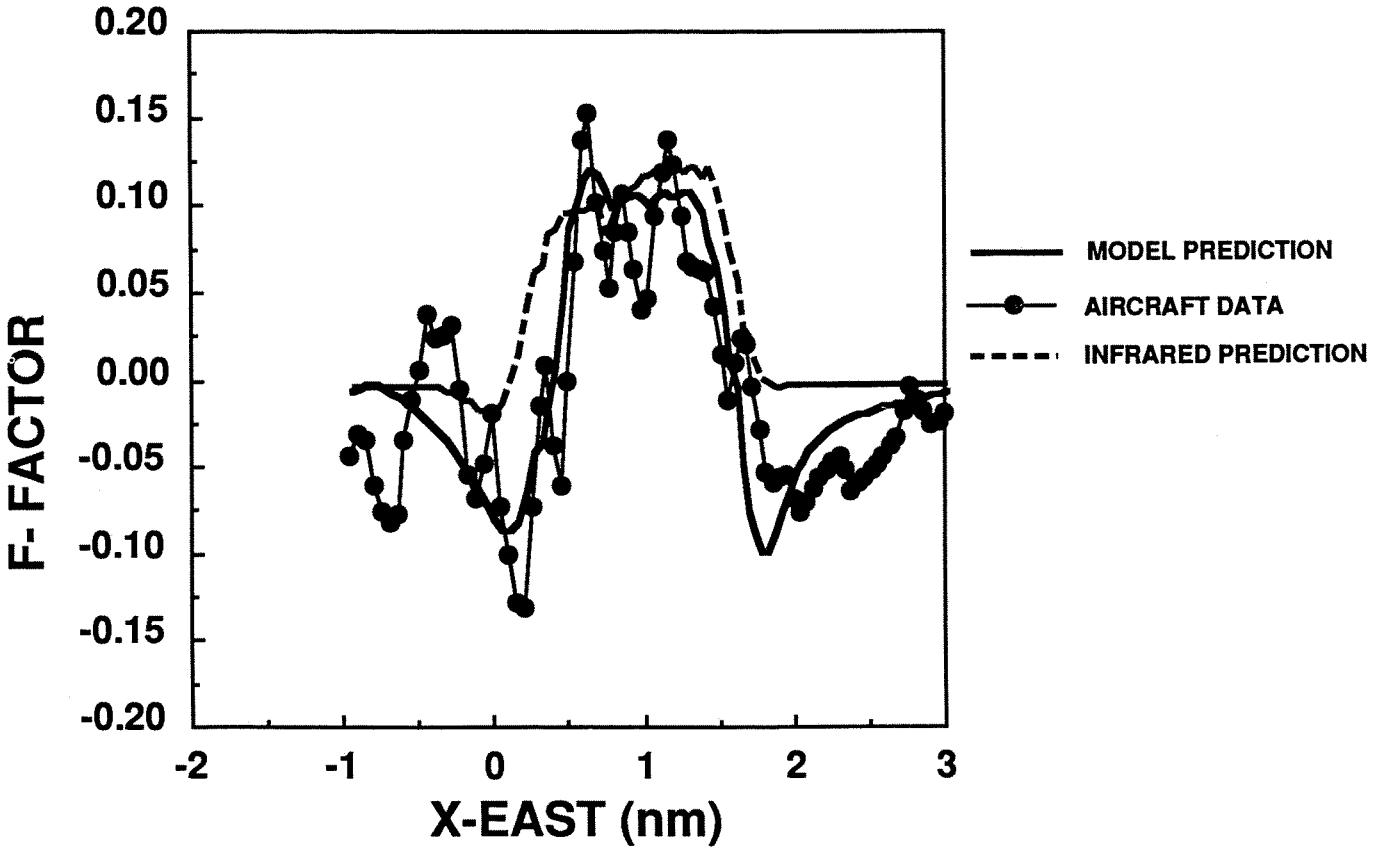

Figure 12. F-Factor comparison between infrared algorithm prediction, aircraft data, and model prediction.

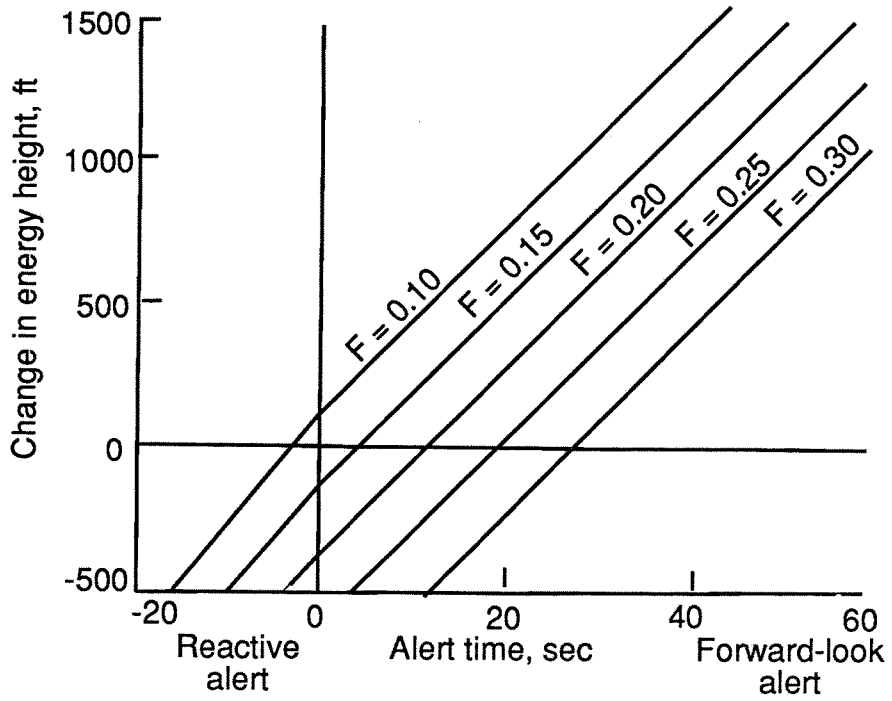

Figure 13. Effect of alert time on airplane energy height during a wind shear encounter.